Topology comparison of slotless permanent magnet semispherical actuators

Topology Comparison of Slotless Permanent Magnet Semispherical Actuators

B. van Ninhuijs, J. W. Jansen, B. L. J. Gysen, and E. A. Lomonova

Department of Electrical Engineering, Eindhoven University of Technology, Eindhoven 5612 AZ, The Netherlands

This paper presents a comparison of several three-degrees-of-freedom (DoFs) semispherical actuator topologies, which can mimic a shoulder joint of an actuated support system. A semianalytical model is applied to determine the torque performance as function of the position. Hence, the current distribution through the coils with minimized ohmic losses can be determined. The performed topology comparison is based on the average power dissipation and on a set of torque and range of motion requirements.

***Index Terms*— Actuated support systems, spherical actuator, spherical permanent magnet array.**

I. Introduction

ACTUATED support systems are used by people with diminished arm activities to increase the quality of life. The more actuated degrees of freedom (DoFs), the more support can be provided. To mimic the shoulder joint and cover the range of motion of a human arm, at least three DoFs are required. These DoFs can be achieved with several stacked single-DoF actuators, however, this results in large and cumbersome constructions [1]. As arm support systems are often mounted on an electric wheelchair, these systems must be flexible, lightweight and have a low energy consumption. Therefore, a three-DoF semispherical actuator is proposed.

Existing prototypes of spherical actuators consider a full spherical permanent magnet array [2]–[5]. Due to the construction of the arm support system, the actuator design is mechanically limited to a semispherical permanent magnet array. Hence, end effects will influence the optimal combination of the coil topology, coil array, and magnet array.

This paper discusses several semispherical actuator topologies and compares the performance based on the average power dissipation. First, the applied semianalytical model and the applied current–torque decoupling are presented. Second, the investigated coil topologies, coil arrays, and semispherical permanent magnet arrays are shown. Third, the obtained average power dissipation results are analyzed and compared.

II. Comparison Method

A. Requirements

To assist the user with the basic activities of daily living, a set of requirements is deducted in [1]. During these basic tasks, a range of motion from $-45°$ to $45°$ is desired about the x-axis, y-axis, and z-axis. The required continuous torque, to achieve the accelerations during the tasks of daily living, is around 4 N m over the complete range of motion.

Manuscript received March 7, 2014; accepted May 26, 2014. Date of current version November 18, 2014. Corresponding author: B. van Ninhuijs (e-mail: b.v.ninhuijs@tue.nl).

Color versions of one or more of the figures in this paper are available online at http://ieeexplore.ieee.org.

Digital Object Identifier 10.1109/TMAG.2014.2329180

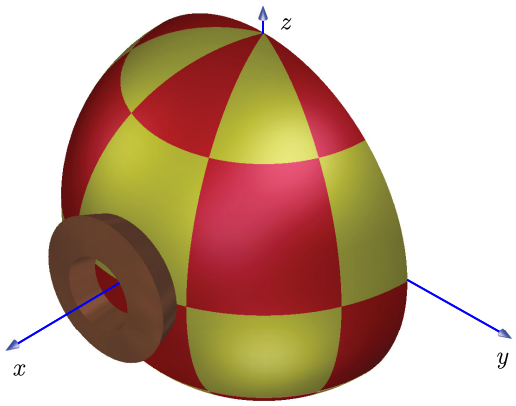

Fig. 1. Spherical actuator topology used for validation of the analytical model.

B. Power Dissipation

The magnetic flux density, of the semispherical permanent magnet array, in combination with the current through the coils determines the torque performance. The magnetic flux density can be calculated with the magnetic charge model (MCM), as presented in [6]. Defining a current, through a slotless coil topology, for example, as shown in Fig. 1, the torque can be determined with the Lorentz force law

$$\vec{T} = \int \vec{r} \times \vec{J} \times \vec{B} \ \mathrm{dV} \tag{1}$$

where $\vec{r}$ is the displacement vector, $\vec{J}$ is the current density, and $\vec{B}$ is the magnetic flux density. This semianalytical model is validated by comparing the torque results of the actuator topology, as shown in Fig. 1 with 3-D finite element analysis (FEA). These torque results are shown in Figs. 2 and 3 and it can be concluded that both models are within 3% error with each other. This error is calculated with

$$\epsilon = \frac{\max(|T_{\mathrm{FEA}} - T_{\mathrm{MCM}}|)}{\max(T_{\mathrm{FEA}})}. \tag{2}$$

A balanced three-phase coil distribution cannot be obtained due to the end effects, range of motion, and different magnet sizes due to the spherical shape. Furthermore, the torque results, as shown in Figs. 2 and 3, have a nonsinusoidal

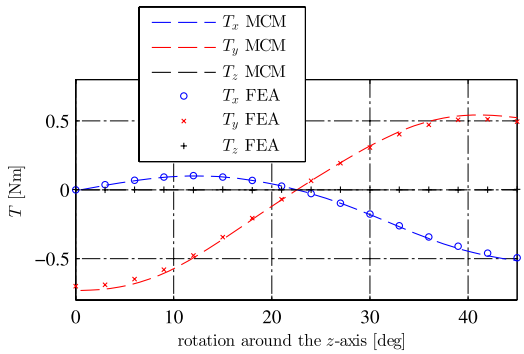

Fig. 2. Comparison of the FEA model and MCM rotating the coil about the z-axis.

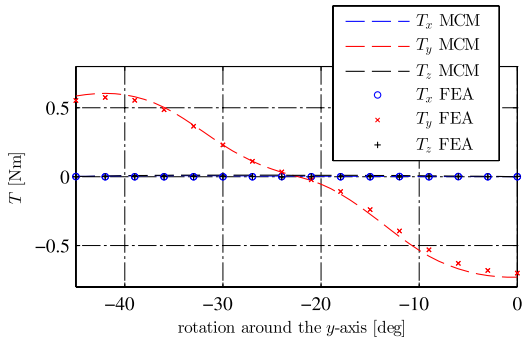

Fig. 3. Comparison of the FEA model and MCM rotating the coil about the y-axis.

behavior with respect to position. Therefore, the current is decoupled from the torque by mapping the currents through the coils for each position, which is defined as [7]

$$\vec{T} = \begin{bmatrix} T_x \\ T_y \\ T_z \end{bmatrix} = \begin{bmatrix} \Gamma_{1,x} & \Gamma_{2,x} & \dots & \Gamma_{n,x} \\ \Gamma_{1,y} & \Gamma_{2,y} & \dots & \Gamma_{n,y} \\ \Gamma_{1,z} & \Gamma_{2,z} & \dots & \Gamma_{n,z} \end{bmatrix} \begin{bmatrix} i_1 \\ i_2 \\ i_3 \\ \vdots \\ i_n \end{bmatrix} \tag{3}$$

$$= \mathbf{\Gamma}(R_x, R_y, R_z)\vec{i} \tag{4}$$

where $\vec{T}$ is the produced torque, $\mathbf{\Gamma}_{l,k}$ is the current mapping for coil l about the k-axis, and i_l is the current through coil l. A two-norm minimization of the current is applied to minimize the ohmic losses and, consequently, minimize the power dissipation. With this method and denoting the desired torque to $\vec{T}_d$, the current can be obtained by

$$\vec{i} = (\mathbf{\Gamma}^\top(\mathbf{\Gamma}\mathbf{\Gamma}^\top)^{-1})\vec{T}_d. \tag{5}$$

III. Topologies

A. Spherical Permanent Magnet Arrays

The amount of magnets in the semispherical permanent magnet array influences the torque performance. Therefore, three semispherical permanent magnet arrays, with a pole pitch of $\tau_m = 45°$, $\tau_m = 36°$, and $\tau_m = 30°$, are included for the comparison and shown in Fig. 4. Symmetry of the semispherical permanent magnet about the z-axis is applied to reduce the end effects, as the magnet array starts and ends

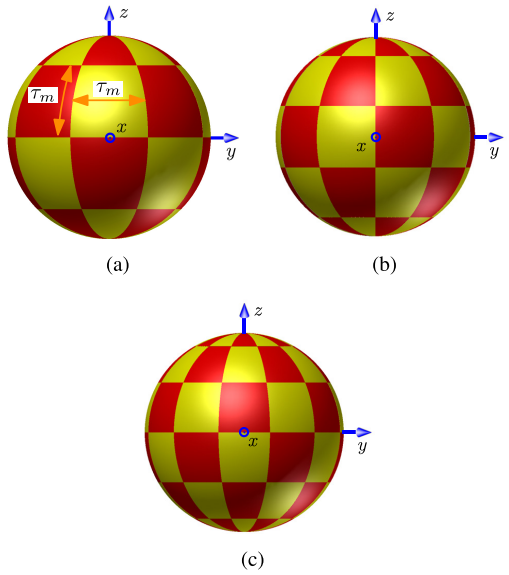

Fig. 4. Investigated semispherical permanent magnet arrays. (a) $\tau_m = 45°$. (b) $\tau_m = 36°$. (c) $\tau_m = 30°$.

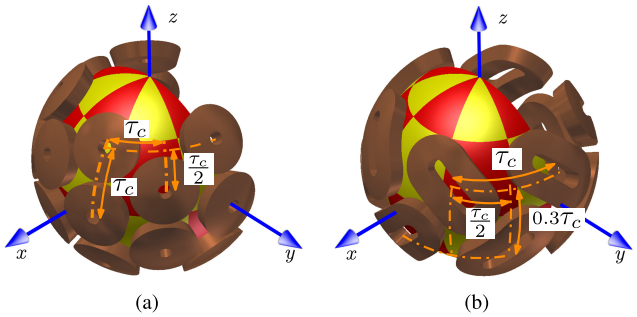

Fig. 5. Investigated coil array topologies. (a) Circular coil array. (b) Elongated coil array.

with a magnet half the width compared with the other magnets as can be observed in Fig. 1.

B. Coil Arrays

Two coil topologies are investigated, namely, circular and elongated coil topologies. The circular coil topology is often used in combination with a spherical permanent magnet array [2], [3], [5], [8] and the elongated coil topology is applied in a comparable planar actuator [9]. The applied coil arrays are shown in Fig. 5 with the geometrical dimensions, as shown in Table I and Fig. 6. Both coils have a spherical shape to keep the air-gap constant at $g = 1$ mm and the geometry variables are defined in degrees. To obtain the optimal ratio between pole pitch and coil pitch, the comparison is made by varying the coil pitches for each defined semispherical permanent magnet array. To comply with the range of motion, both coil arrays have two different mechanical constructions, which are shown in Fig. 7(a) and (b) for the circular and elongated coil array, respectively.

The ratio between the gap G_w and the conductor bundle C_w is set to 25% which results in

$$G_w = \frac{1}{4}C_w. \tag{6}$$

TABLE I
GEOMETRY VARIABLES AND PARAMETERS

Variable	Symbol/Value	Unit
Coil pitch	τ_c	rad
Pole pitch	τ_m	rad
Coil width	C_w	rad
Halve coil gap width	G_w	rad
Halve coil gap length	G_l	rad
Parameter		
Outer radius of the magnet array	64	mm
Outer radius of the coil array	75	mm
Magnet thickness	9	mm
Coil thickness	10	mm
Airgap length	1	mm
Remanent magnetic flux density	1.23	T
Assumed magnet relative permeability	1	-
Rotation of the elongated coils, α	45	deg

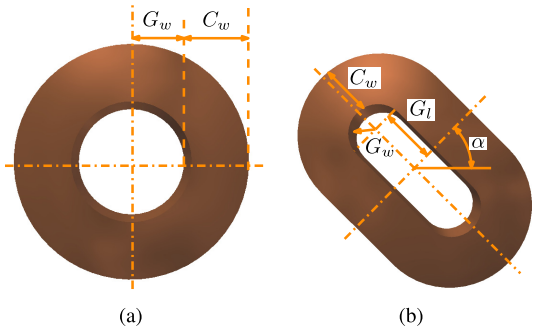

Fig. 6. Coil topologies and their geometric variables. (a) Circular coil. (b) Elongated coil.

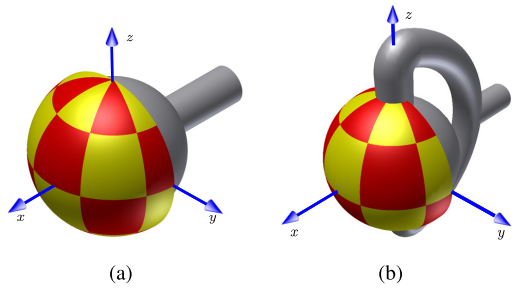

Fig. 7. Mechanical rotor designs for (a) circular coil array and (b) elongated coil array.

For the circular coil array, a combination of two and three layers of coils is considered, as shown in Fig. 5(a). To avoid overlapping of the coils of the third and second layer due to the spherical shape, the width of the coils needs to be corrected which results in

$$G_w + C_w = \tau_c \sin\left(\frac{\pi}{2} - \frac{\tau_c}{2}\right) \tag{7}$$

where τ_c is the coil pitch.

The elongated coil array considers two layers of coils, the top and bottom layer, which are rotated by $\alpha = 45°$ and $\alpha = -45°$, respectively, as shown in Fig. 5(b). The width of these coils is obtained by

$$G_w + C_w = \frac{1}{4}\tau_c \tag{8}$$

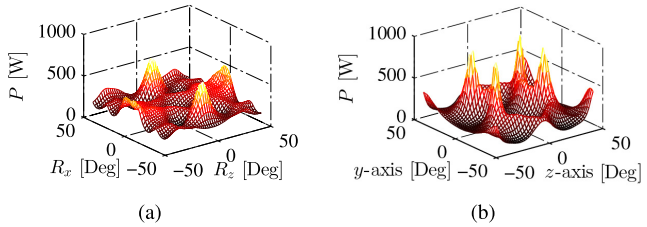

Fig. 8. Power dissipation rotating the coil array, $\tau_c = 37°$ and $\tau_m = 45°$, around the y-axis and z-axis with the torque requirement of (a) $T_x = 4$ N m and (b) $T_y = 4$ N m.

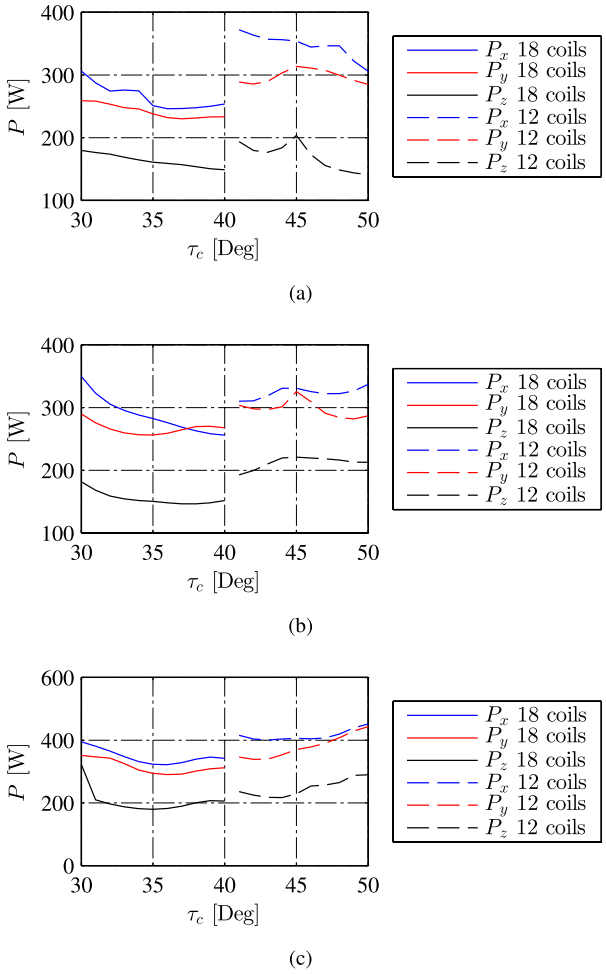

Fig. 9. Average power dissipation of the circular coils for (a) $\tau_m = 45°$, (b) $\tau_m = 36°$, and (c) $\tau_m = 30°$.

where G_w is the elongated coil gap width. The elongated gap length G_l is calculated such that there is as little space as possible between the top and bottom coils, which results in

$$G_l = \frac{\tau_c}{\sin(\alpha)} - 2\,C_w G_w. \tag{9}$$

Considering only the rotations about the y-axis and z-axis, the power dissipation of the configuration shown in Fig. 5(a) is obtained and shown in Fig. 8. In this figure, several peaks are visible that indicate the positions of the array with a low torque performance. For the comparison of all three DoFs, the power dissipation is averaged over the specified range of motion.

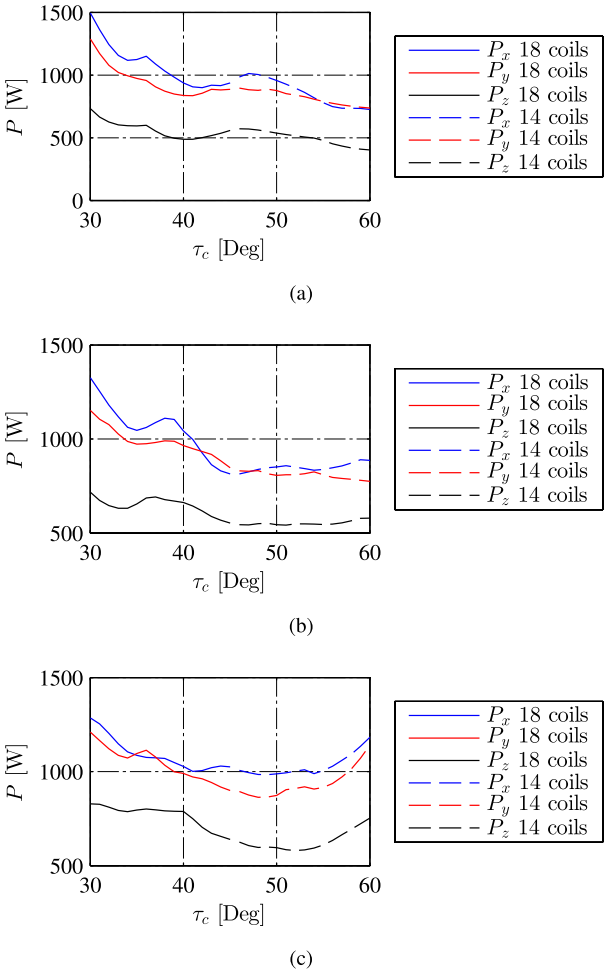

Fig. 10. Average power dissipation of the elongated coils for (a) $\tau_m = 45°$, (b) $\tau_m = 36°$, and (c) $\tau_m = 30°$.

IV. Results

The average power dissipation is calculated for three different torque setpoints (T_x, T_y, T_z) namely, (4, 0, 0), (0, 4, 0), and (0, 0, 4) N m. The power dissipation is shown in Figs. 9 and 10 of the circular and elongated coil topologies, respectively.

To guarantee the range of motion, six coils of the circular coil topology, as shown in Fig. 5(a), which do not completely cover the permanent magnet array were removed during the simulation for a coil pitch higher than 40°. This results in two coil pitch ranges, namely, $30° \leq \tau_c \leq 40°$ and $41° \leq \tau_c \leq 50°$ with 18 coils and 12 coils, respectively. The change in power dissipation as function of τ_c, visible in Fig. 9, decreases for smaller pole pitch τ_m. Furthermore, it shows that for larger magnet arrays the transition is smoother from a 18 coil array to a 12 coil array. The most optimal topology for the circular coil array is the $\tau_c = 37°$ and $\tau_m = 45°$, as observed in Fig. 8.

The coil pitch of the elongated coil array as shown in Fig. 5(b) is limited at 45°, otherwise they will overlap. This results in two coil pitch ranges, namely, $30° \leq \tau_c \leq 45°$ and $46° \leq \tau_c \leq 60°$ with 18 coils and 14 coils, respectively. By removing the four coils at the back side of the semispherical permanent magnet array, the change of coil array size has almost no influence on the power dissipation, as shown in Fig. 10. A large ratio of the coil pitch to the pole pitch is desired as can be observed in Fig. 10(a) and (b), however, at a certain point, the power dissipation will increase again, as shown in Fig. 10(c). The most optimum combination for the elongated coil topology is $\tau_c = 60°$ and $\tau_m = 45°$.

The maximum rotation about the x- and y-axis of the elongated coil topology cause high power dissipation peaks, which results in a relative high average power dissipation in comparison with the circular coils. These positions should be avoided to decrease the total power consumption. From comparison between the circular coils and elongated coils, it can be concluded that the circular coil array clearly outperforms the elongated coil array for the considered permanent magnet arrays and motion profiles. Finally, from these results, a conclusion on the optimum semispherical actuator is given.

V. Conclusion

The power dissipation has been analyzed for several combinations of coil arrays and semispherical permanent magnet arrays. A semianalytical method, which has been verified with FEA, has been applied. A two-norm minimization of the currents through the coils has been obtained and, subsequently, the average minimized power dissipation. From this analysis, it has been concluded that there is an optimal semispherical actuator topology, namely: $\tau_c = 37°$ and $\tau_m = 45°$, utilizing the circular coil topology for the considered permanent magnet arrays and motion profiles.

Acknowledgment

This work was supported by the Dutch Pieken in de Delta Program under Project McArm PID102055.

References

[1] B. van Ninhuijs, L. van der Heide, J. W. Jansen, B. L. J. Gysen, D. J. van der Pijl, and E. A. Lomonova, "Overview of actuated arm support systems and their applications," *Actuators*, vol. 2, no. 4, pp. 86–110, Oct. 2013.

[2] L. Yan, I.-M. Chen, G. Yang, and K.-M. Lee, "Analytical and experimental investigation on the magnetic field and torque of a permanent magnet spherical actuator," *IEEE/ASME Trans. Mechatron.*, vol. 11, no. 4, pp. 409–419, Aug. 2006.

[3] T. Yano, "Proposal of a truncatedoctahedron-dodecahedron based spherical stepping motor," in *Proc. 19th Int. Conf. Elect. Mach., ICEM*, Sep. 2010, pp. 1–6.

[4] W. Wang, J. Wang, G. W. Jewell, and D. Howe, "Design and control of a novel spherical permanent magnet actuator with three degrees of freedom," *IEEE/ASME Trans. Mechatron.*, vol. 8, no. 4, pp. 457–468, Dec. 2003.

[5] K. Kahlen, I. Voss, C. Priebe, and R. W. D. Doncker, "Torque control of a spherical machine with variable pole pitch," *IEEE Trans. Power Electron.*, vol. 19, no. 6, pp. 1628–1634, Nov. 2004.

[6] B. van Ninhuijs, T. E. Motoasca, B. L. J. Gysen, and E. A. Lomonova, "Modeling of spherical magnet arrays using the magnetic charge model," *IEEE Trans. Magn.*, vol. 49, no. 7, pp. 4109–4112, Jul. 2013.

[7] J. W. Jansen, C. M. M. van Lierop, E. A. Lomonova, and A. J. A. Vandenput, "Magnetically levitated planar actuator with moving magnets," *IEEE Trans. Ind. Appl.*, vol. 44, no. 4, pp. 1108–1115, Jul./Aug. 2008.

[8] K.-M. Lee and H. Son, "Distributed multipole model for design of permanent-magnet-based actuators," *IEEE Trans. Magn.*, vol. 43, no. 10, pp. 3904–3913, Oct. 2007.

[9] J. M. M. Rovers, J. W. Jansen, and E. A. Lomonova, "Multiphysical analysis of moving-magnet planar motor topologies," *IEEE Trans Magn.*, vol. 49, no. 12, pp. 5730–5741, Dec. 2013.